Theor Chem Account (2008) 121:271–278
DOI 10.1007/s00214-008-0474-z

REGULAR ARTICLE

The interconversion mechanism between TcO^{3+} and TcO_2^{+} core of ^{99m}Tc labeled amine-oxime (AO) complexes

Hong-Mei Jia · De-Cai Fang · Yan Feng · Jian-Ying Zhang · Wen-Bo Fan · Lin Zhu

Received: 15 June 2008 / Accepted: 8 August 2008 / Published online: 2 September 2008

Abstract Density functional theory, employing B3LYP/DZVP and B3LYP/6-31G*(LANL2DZ for Tc), has been used to investigate the interconversion mechanism between formal TcO^{3+} and TcO_2^{+} core of ^{99m}Tc labeled amine-oxime (AO) complex, in which two water molecules have been used to simulate the possible interconversion process. The obtained results indicate that the length of amine-amine hydrocarbon backbone of AO ligand has a significant influence on the stabilities of formal TcO^{3+} and TcO_2^{+} complex. The interconversion process between TcO–BnAO and TcO_2–BnAO has been amply discussed, which releases the useful information for the further investigation of the structure and hypoxic mechanism of ^{99m}Tc-HL91.

Keywords Interconversion mechanism · TcO^{3+} core · TcO_2^{+} core · ^{99m}Tc-HL91 · B3LYP

Electronic supplementary material The online version of this article (doi:10.1007/s00214-008-0474-z) contains supplementary material, which is available to authorized users.

H.-M. Jia · D.-C. Fang (✉) · Y. Feng · J.-Y. Zhang · W.-B. Fan · L. Zhu
Key Laboratory of Radiopharmaceuticals, Ministry of Education, College of Chemistry, Beijing Normal University, 100875 Beijing, People's Republic of China
e-mail: dcfang@bnu.edu.cn

L. Zhu
e-mail: zhulin@bnu.edu.cn

1 Introduction

^{99m}Tc labeled amine-oxime (AO) complexes have been extensively studied in order to develop ^{99m}Tc radiopharmaceuticals for the measurement of regional cerebral blood flow. ^{99m}Tc-d,l-HMPAO are found to be the first ^{99m}Tc labeled brain perfusion imaging agent approved by FDA [1]. Later, ^{99m}Tc-HL91 (^{99m}Tc-BnAO) has been evaluated as a tissue hypoxia imaging agent [2–8], and it was reported that the intrinsic properties of the ^{99m}Tc-HL91 were predominately responsible for the hypoxia selectivity [2], not the uncomplexed HL91 ligand [4]. But until now, the structure and hypoxic mechanism of ^{99m}Tc-HL91 are still not clear. It is interesting that these technetium(V) amine oxime complexes showed both five-coordinate monooxo technetium(V) spicies and six-coordinate trans-dioxo technetium(V) spicies, in which the former has the formal oxidation state of TcO^{3+} and the latter has the formal oxidation state of TcO_2^{+}. The length of amine-amine hydrocarbon backbone of AO ligand has significant influence on the formation of formal TcO^{3+} or TcO_2^{+} complex [9–12]. Moreover, the syn and anti isomers of ^{99m}TcO(PnAO-6-R) can interconvert in the presence of water, in which $^{99m}TcO_2$(PnAO-6-R) intermediate could be formed [13]. It was also reported that ^{99}Tc-HL91 could in solution adopt both the penta-coordinated mono-oxo form and hexa-coordinated di-oxo form [14], but it is still uncertain which form is related to the uptake mechanism of ^{99m}Tc-BnAO. Brauers et al. [14] suggested that the uptake mechanism of this compound might be related to the interconversion of these two forms. However, no evidence from the experiments has been established for this assumption up to now. It is essential from theoretical calculation to elucidate the probable interconversion mechanism between formal TcO^{3+} and TcO_2^{+} core of

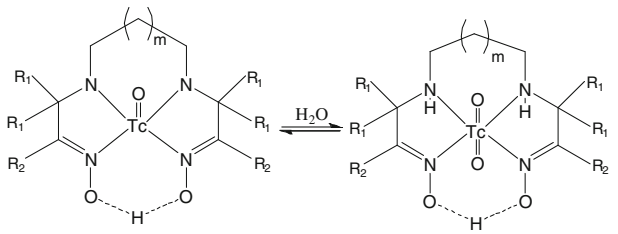

	a	b	c	d	e
m	1	2	2	2	3
R_1	H	H	CH_3	CH_3	H
R_2	H	H	CH_3	H	H

Scheme 1 The studied reactions

^{99m}Tc-AO, which is useful for understanding the structures and hypoxic mechanisms of these applicable compounds. The studied reactions are shown in Scheme 1, in which both five-coordinate monooxo technetium(V) complex 1 and six-coordinate trans-dioxo technetium(V) complex 2 are neutral.

2 Methods of calculations

The Becke-3 Lee-Yang Parr (B3LYP) method [15, 16] was used in all calculations in this work, using the Gaussian 03 program package [17]. In order to accurately and quantitatively characterize the electron structure, it was essential to use all-electron wavefunctions for the analysis of quantum theory of atoms in molecules (QTAIM) [18, 19], for which the DZVP basis set [20] was employed in-place of a effective core potential (ECP) basis set, such as LANL2DZ [21] in Gaussian program. The geometries of reactants, products, complexes, intermediates and transition states were fully optimized with B3LYP/DZVP method to the convergences criteria of 3.0×10^{-4}, 4.5×10^{-4}, 1.2×10^{-3}, 1.8×10^{-3} as acceptance thresholds for the gradients of the root mean square (RMS) force, maximum force, RMS displacement and maximum displacement vectors, respectively. LANL2DZ basis set has also been employed for Tc atom and 6–31G(d) basis sets have been used for other atoms for comparison.

Structures residing at minima or maxima (stationary points) on the potential energy surface (PES) of this reaction, have been located and characterized by their number of imaginary frequencies, at the B3LYP/DZVP level of theory, except where noted elsewhere. Intrinsic reaction coordinate (IRC) [22–24] computations were used to trace the reaction paths to confirm that the TS structures obtained corresponded to the two adjacent minima proposed as lying on either side of that TS. The infrared spectral results showed that Tc-O stretching vibration of TcO_2–BnAO [12] and TcO–PnAO [10] were 784 and 923 cm^{-1}, and calculated values were 825 and 963 cm^{-1}, from which one can derive that the scaling factor is 0.95 that was comparable with 0.96 for B3LYP/6-31G(d) calculation [25, 26]. The relative energies of all structures found at these stationary points were corrected with their corresponding zero-point vibrational energies (ZPE) scaled by 0.95.

The solvent effects of the title reactions have been performed with the PCM model [27–33] with water ($\varepsilon = 78.39$) as solvent at a temperature of 298 K, denoted as SCRF-B3LYP/DZVP. Water molecules are used not only as solvents, but also as the reactants for the interconversion process of formal TcO^{3+} and TcO_2^{+} complexes. For the reaction of TcO–BnAO + $2H_2O$ → TcO_2–BnAO + H_2O, SCRF-B3LYP/DZVP method has been employed to optimize the structure parameters of the reactants, complexes, intermediates, transition states and products, and thus obtained geometries have been characterized with the vibrational analysis at the same calculation level.

In the light of the QTAIM approach, critical points (CPs) of rank 3 were identified in the electron densities, obtained at B3LYP/DZVP level of theory. There are bond critical points (BCPs), ring critical points (RCPs) and cage critical points (CCPs). The existence of a BCP between two atoms in an equilibrium molecular geometry is the necessary condition for two atoms that are bonded to one another. The pairs of gradient paths that originate a BCP and terminate at neighboring nuclei define a line through which electron distribution, $\rho(\mathbf{r})$, is a maximum with respect to any lateral displacement. In this paper, BCP properties were obtained using AIMPAC [34, 35] and AIM98PC [36], and the molecular graphs were studied and plotted with AIM2000 [37, 38].

3 Results and discussions

3.1 The stability of TcO_2-core

It was well-known that the length of amine-amine hydrocarbon backbone of AO ligand has a significant influence on the formation of formal TcO^{3+} or TcO_2^{+} complex [9–12]. Previous experiments have confirmed that ligands EnAO (see Scheme 1, $m = 0$, R_1=R_2=CH_3) and PnAO (see Scheme 1, $m = 1$, R_1=R_2=CH_3) give a five coordinate, monooxo technetium complexes, while ligand PentAO (see Scheme 1, $m = 3$, R_1=R_2=CH_3) provided six coordinate, dioxo core complex. However, it is not clear whether the structure of Tc–BnAO (see Scheme 1, $m = 2$,

Table 1 The chief geometric parameters (bond length in Å) of **1** and **2** optimized with different basis sets both in gas phase and in water (see Scheme 2 for the atomic numbering systems)

	Tc1–O2	Tc1–O10	Tc1–N5	Tc1–N6	Tc1–N3	Tc1–N4	O7–O8	N3–N4
1a	1.698[a]	–	2.132	2.156	1.969	1.953	2.497	2.803
	1.720[b]		2.132	2.148	1.958	1.945	2.520	2.799
	1.690[c]		2.122	2.144	1.957	1.941	2.491	2.789
	1.708[d]		2.122	2.136	1.946	1.935	2.499	2.785
2a	1.781	1.773	2.076	2.132	2.257	2.172	2.894	3.411
	1.783	1.783	2.103	2.157	2.229	2.160	3.098	3.362
	1.768	1.759	2.060	2.105	2.246	2.165	2.785	3.408
	1.769	1.768	2.079	2.117	2.215	2.153	2.831	3.379
1b	1.698	–	2.146	2.146	1.986	1.964	2.477	2.888
	1.719		2.147	2.137	1.972	1.953	2.508	2.884
	1.690		2.138	2.132	1.973	1.950	2.467	2.869
	1.708		2.138	2.124	1.962	1.942	2.500	2.866
2b	1.775	1.770	2.085	2.129	2.339	2.221	2.656	3.686
	1.781	1.781	2.100	2.133	2.297	2.207	2.690	3.623
	1.761	1.757	2.075	2.113	2.332	2.216	2.626	3.679
	1.766	1.764	2.088	2.116	2.295	2.203	2.647	3.624
1e	1.695	–	2.150	2.171	1.991	1.975	2.455	2.982
	1.717		2.151	2.165	1.978	1.965	2.473	2.976
	1.688		2.142	2.160	1.978	1.963	2.443	2.968
	1.706		2.142	2.154	1.968	1.954	2.462	2.962
2e	1.772	1.767	2.087	2.135	2.379	2.266	2.602	3.830
	1.779	1.779	2.101	2.137	2.323	2.251	2.625	3.755
	1.758	1.755	2.078	2.118	2.371	2.263	2.578	3.824
	1.763	1.763	2.089	2.119	2.323	2.251	2.595	3.757

[a] B3LYP/DZVP

[b] SCRF-B3LYP/DZVP

[c] B3LYP/6-31G(d) (LANL2DZ for Tc)

[d] SCRF-B3LYP/6-31G(d) (LANL2DZ for Tc)

R_1=R_2=CH_3) will adopt monooxo or dioxo core form. Therefore, the characterizations of their structures and stabilities from DFT calculation will provide valuable information.

The main geometric parameters of **1** and **2** optimized with different basis sets in gas phase and in water are listed in Table 1, from which one can observe that the geometric alterations for different basis sets and different media are not noticeable. For example, the differences for bond lengths of Tc–O and Tc–N are within 0.02 Å. Even for the distances of O···H–O and N···N, the basis set effect is still small. However, the solvent H_2O has some influence on small ring system ($m = 1$), and the biggest difference for the distance of O···O reaches 0.204 Å. For species **1**, the group Tc=O is on the top of plane of NNNN, forming a pyramid structure; while for species **2**, Tc atom is almost on the same plane with NNNN. This may cause the different stability of formal TcO_2^+ core in different ring lengths as shown in Table 2. The interpretation for these results is that the approaching of Tc atom to NNNN plane will cause the expansion of ring to reduce the repulsion between these groups, through increasing the N–Tc–N angle and thus N–N distances, which in turn increase the distance of O···H–O. For $m = 3$, the distance of O···H–O in formal TcO_2^+ core is very close to that in formal TcO^{3+} core; while for $m = 1$, the distance of O···H–O in formal TcO_2^+ core is about 0.4 Å longer than that in formal TcO^{3+} core. Such alteration will change the strength of O···H–O, which can be observed from change of the electron density at bond critical point (ρ_b), as illustrated in Fig. 1. It can be observed that values of ρ_b for the O···H in **1a** and **2a** are 0.083 and 0.018 au, respectively, which reveals that the strength of O···H–O becomes very weak in **2a**, and it is too unstable to be isolated from the experiments. The hydrogen-bonding energy can be estimated to be about 12.3 kcal/mol, with the calculated energy difference between **1a** and an isomer of **1a** that the hydrogen atom is turned aside from O···H–O. The hydrogen-bonding

Table 2 The relative energies (kcal/mol) of TcO_2–AO relative to TcO–AO + H_2O

	B3LYP	B3LYP + 0.95ZPE	SCRF–B3LYP	SCRF–B3LYP + 0.95ZPE
2a	17.1[a]	23.2	10.8	16.6
	12.3[b]	18.6	6.2	12.3
2b	−4.0	2.4	−8.3	−2.0
	−9.3	−2.9	−13.8	−7.6
2c	−3.6	2.7	−4.5	2.1
	−8.8	−2.4	−9.8	−3.2
2d	−5.7	0.6	−6.3	0.1
	−10.9	−4.7	−11.8	−5.5
2e	−7.0	−1.0	−9.8	−4.0
	−12.1	−6.1	−15.2	−9.3

[a] DZVP

[b] 6-31G(d), except LANL2DZ for Tc

energy in **2a** is only 1.7 kcal/mol with the same calculation method. Therefore, the loss of hydrogen-bonding is the main contribution to the destabilization of **2a**.

From the structures of 1 and 2 in Scheme 1, one can break two OH bonds and two R_2N–(TcO) bonds in the reactant; while one can also make two NH bonds, one Tc=O bond and two dative R_2HN–(TcO_2) bonds in the product. In order to estimate the energy change, the following five reactions have been designed: (1) $H_2O \rightarrow 2H + O$; (2) $(CH_3)_2\,NH \rightarrow (CH_3)_2\,N + H$; (3) $TcO_2 \rightarrow TcO + O$; (4) $(CH_3)_2\,N$–(TcO) → TcO + $(CH_3)_2N$; (5) $(CH_3)_2NH$–(TcO_2) → TcO_2 + $(CH_3)_2NH$. B3LYP/DZVP calculations, plus the ZPE with 0.95 scaling factor, indicate that the reaction heats for above five reactions are 233, 100, 127, 70 and 38 kcal/mol, respectively, from which one can work out that the reaction releases energy of about 30 kcal/mol. Although this is a very coarse estimation, in which one ignores the ring distortion, the repulsion between atoms in the ring and TcO or TcO_2 and the change of O–H···O bonding, it is still helpful for understanding the reaction process.

In addition, the basis sets have some influence on the geometric parameters and energetics. The bond lengths related to Tc obtained with LANL2DZ are shorter than those optimized with DZVP basis set (see Table 1) and the LANL2DZ basis set probably overestimates the stability of complex 2, which is about 5 kcal/mol from the data in Table 2. It can be explained that LANL2DZ basis set might give less repulsion between Tc atom and N or O atoms due to the frozen core electrons. Therefore, only DZVP results have been discussed afterward.

3.2 The interconversion mechanism of formal TcO^{3+} and TcO_2^{+}

All the possible stationary points along the reaction paths have been located and verified. The main atomic numbering systems of the possible stationary points are shown in Scheme 2, in which two water molecules are involved in the interconversion process. It is clear that the proposed interconversion process has two distinctive steps, i.e., the addition of two water molecules and the leaving of one water molecule (from **1** to **INT1**), and proton transfer with the aid of one water molecule (from **INT1** to product **2**). Not only the water molecules are as reactants, but also the water molecules are acted as solvent that has certain effect to the interconversion reaction. As the real reactions take place in water solution, the following discussions are based on SCRF-B3LYP calculations, except noted otherwise.

The chief geometrical parameters (bond length in Å) for transition states and intermediate, optimized in both gas phase and water solution, are listed in Table 3, from which one can see that the geometric parameters optimized with different media are quite similar for $m = 2$ case. For the first addition step, the reaction proceeds to **INT1b** via transition state **TS1b**, a six-membered loose ring structure in addition portion, in which the bond length of the forming Tc–O is still about 0.6 Å longer than that in **2b** (comparing Tables 1 and 3) and the bond lengths of O14···H13 and N3···H11 in this ring are within the range of 1.2–1.5 Å. The intermediate **INT1b** adopts TcO(OH) form, in which Tc–OH is a typical single bond and the whole big ring is expanded as the Tc atom sits in the plane of NNNN. Since the energy for the species that a water molecule sticks on **INT1b** is almost the same as those of **INT1b** + H_2O, it is reasonable to speculate that the forming water molecule will leave **INT1b** and enter water solution. **INT1b** will finish the proton transfer from TcO(OH) to N atom with the aid of one water molecule via a transition state **TS2b**, in which the Tc-O bonding is in the middle of a double bond and a single bond and the bond distances of O14···H13 and N3···H11 in this ring ranges from 1.2 to 1.5 Å. Here this water molecule is like as a catalyst, and it will be recovered and enter into water solution as the formation of final product **2b**.

The schematic description of the potential energy surface for **1b** + $2H_2O$ is given in Fig. 2l, from which one can observe that product **2b** is a little more stable than reactant **1b**. The energy barriers for the first step and second step are

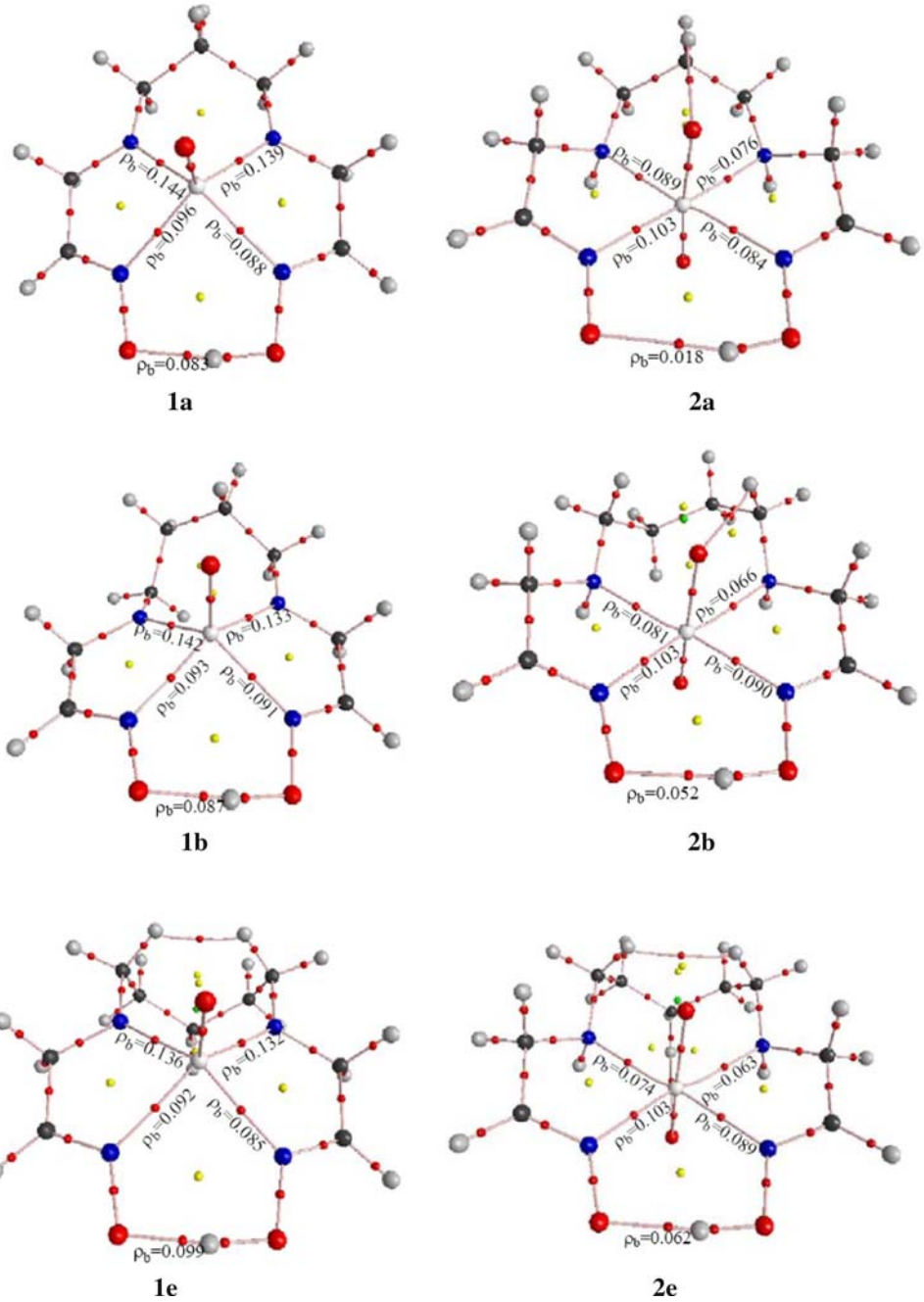

Fig. 1 Molecular graphs, together with the main densities at bond critical points (ρ_b in au). Bond, ring critical and cage points are denoted by *red*, *yellow* and *green dots*, respectively

10.2 and 15.8 kcal/mol, so the second step is the rate-controlling one. The reverse process is also possible as the energy barrier for **2b**–**INT1b** is 22.4 kcal/mol. Once the intermediate **INT1b** is formed, the reaction will proceed to **1b** more easily than back to **2b**, which might be responsible for the structure uncertainty of Tc-HL91. In order to test whether the geometric optimization will change the relative energy obviously or not, single-point SCRF calculations have been performed with optimized geometrics in gas phase for comparison. It turns out that the energy differences for the possible stationary points are all less than 2 kcal/mol, which has been observed for other reactions [39–42].

The potential energy profiles for different ring-lengths are depicted in Fig. 2r, from which one can see that the energies of intermediate **INT1a** and product **2a** are all about 12 kcal/mol above that of **1a**. This thermal instability prevents the interconversion from **1a** to **2a** to take place, which is in good agreement with the experimental fact that only TcO–PnAO crystal could be formed. For $m = 3$ case, the energy barriers for the first step and second step are all close to 10.0 kcal/mol, and **2e** is the most stable one among

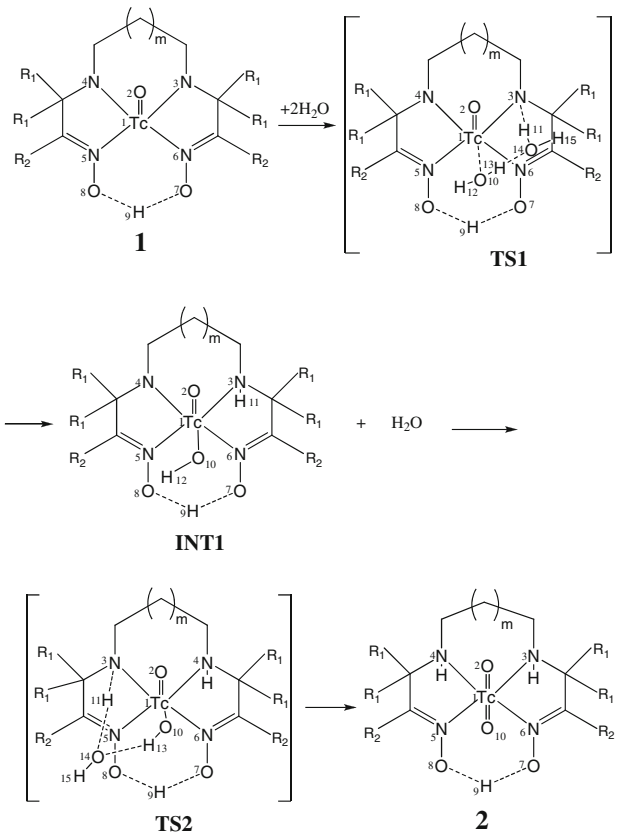

Scheme 2 Typical model of interconversion process for Tc–AO complexes (see Scheme 1 for the different substituents)

our studied systems, which has been confirmed by experiments that the TcO_2–PentAO is isolated. The energy of **INT1e** is almost the same as that of **1e**, and the energy of **TS1e** is also very close to that of **TS2e**. Even if the energy barrier of the reverse process from **2e** to **INT1e** is less than 20 kcal/mol, the possibility for the reverse process is quit low due to the thermal stability of **2e**.

In the real experimental systems, there are six methyl substituents on the backbone, which is also called Tc-HL91. In order to consider the substituent effect, two types of substituent forms (R_1=R_2=CH_3 and R_1=CH_3, R_2=H), as shown in Fig. 2r, have been chosen. From Fig. 2r, one can see that six methyl substituents will increase the relative energies for all the stationary points, especially for **2c**, which leads to that the stability of **2c** is almost the same as that of **1c** (Table 2). Therefore, it turns out that the chance for the interconversion from **2c** to **1c** becomes larger.

In order to verify the above calculation results, the ligand exchange method with Tc-GH intermediate has been employed to obtain the Tc–BnAO complex and analyzed with HPLC. The obtained chart, shown in Fig. 3, indicates that there are three main HPLC peaks, which probably correspond to three forms of Tc–BnAO complexes, i.e., TcO–BnAO, TcO(OH)–BnAO and TcO_2–BnAO. Since the stability of TcO_2–BnAO is relatively higher than that of TcO–BnAO, the peak with retention time 23.40 min in Fig. 3 might be from $^{99m}TcO_2$–BnAO complex. It is well known that ligand exchange method with ^{99m}Tc–GH intermediate will provide the ^{99m}TcO-complex, therefore, there might be one of the peaks in Fig. 3 that comes from TcO–BnAO. As the energy barrier for conversion of TcO(OH)–BnAO to TcO_2–BnAO is about 10 kcal/mol higher than that of TcO–BnAO to TcO(OH)–BnAO, and the stability of TcO_2–BnAO is comparable to that of TcO–

Table 3 The chief geometrical parameters (bond length in Å) for transition states and intermediate of **1** + $2H_2O$ reaction in gas phase except for the reaction of **1b** + $2H_2O$

	Tc1–O2	Tc1–N3	Tc1–N4	Tc1–O10	O10–H13	H13–O14	O14–H11	N3–H11	N3–N4	O7–O8
TS1a	1.696	2.137	1.931	2.393	1.087	1.379	1.372	1.163	2.945	2.776
TS1b	1.694[a]	2.169	1.954	2.388	1.061	1.440	1.307	1.208	3.103	2.641
	1.706[b]	2.158	1.946	2.385	1.053	1.471	1.309	1.213	3.094	2.656
TS1e	1.696	2.194	1.958	2.309	1.066	1.423	1.262	1.255	3.278	2.671
INT1a	1.716	2.192	1.939	2.109	–	–	–	1.029	3.097	2.859
INT1b	1.717[a]	2.275	1.952	2.065	–	–	–	1.024	3.324	2.696
	1.734[b]	2.261	1.937	2.057				1.028	3.285	2.742
INT1e	1.719	2.311	1.959	2.033	–	–	–	1.023	3.461	2.697
TS2a	1.729	2.248	2.085	1.893	1.095	1.392	1.276	1.241	3.316	2.922
TS2b	1.727[a]	2.280	2.107	1.894	1.091	1.400	1.266	1.252	3.493	2.743
	1.723[b]	2.251	2.094	1.924	1.063	1.469	1.292	1.233	3.443	2.776
TS2e	1.724	2.354	2.147	1.890	1.077	1.433	1.248	1.272	3.684	2.620

[a] Gas phase

[b] In water solution

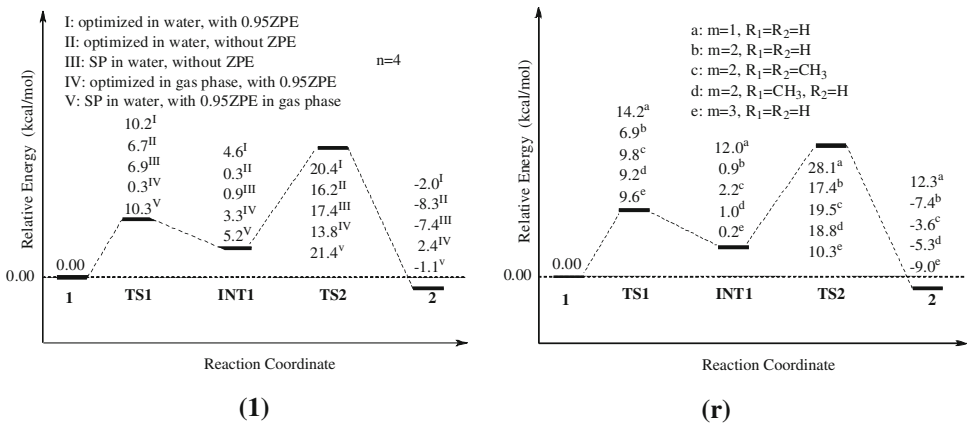

Fig. 2 **l** Schematic description of the potential energy surfaces of **1b** + $2H_2O$ (relative energy in kcal/mol); **r** Schematic description of the potential energy surface of **1** + $2H_2O$ (SP in water, without ZPE) (relative energy in kcal/mol)

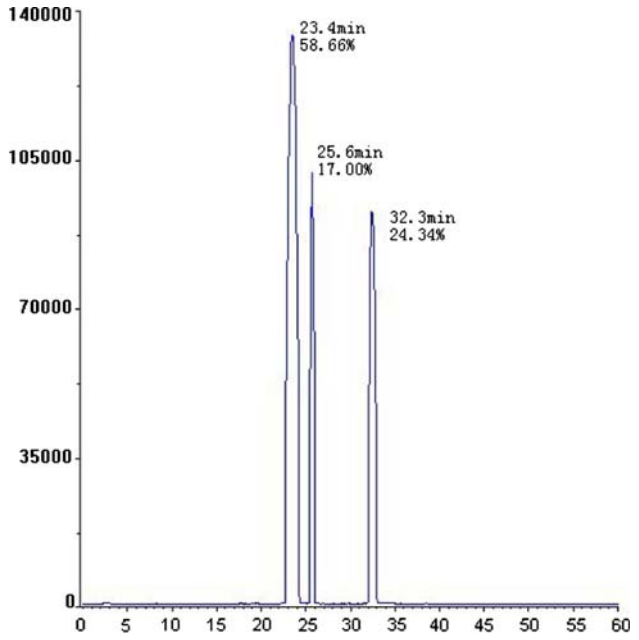

Fig. 3 HPLC chromatograms of ligand exchange method (the mixtures of $^{99m}TcO_2$–BnAO, ^{99m}TcO–BnAO and the ^{99m}TcO(OH)–BnAO intermediate)

BnAO, TcO(OH)–BnAO might coexists with other two forms in water solution.

3.3 The hypoxic mechanism of ^{99m}Tc–BnAO

It was reported that ^{99m}Tc–BnAO showed a selective hypoxic accumulation only at 37 °C and little accumulation at 20 and 4 °C. Moreover, the specific binding of ^{99m}Tc–BnAO may be a slower process than that of BRU59–21 [43]. According to our experience, the lipophilicity of TcO–BnAO may be relatively higher than that of TcO_2–BnAO. If both complexes with formal TcO^{3+} core and TcO_2^{+} core coexist in water, TcO–BnAO will first cross the member into the cell by passive diffusion. The data in Fig. 2 indicate that the conversion process from TcO_2–BnAO to TcO–BnAO is somewhat slow, but the reaction will go quickly toward to TcO–BnAO not back to TcO_2–BnAO once the formation of TcO(OH)–BnAO, which might be related to the hypoxic mechanism of ^{99m}Tc–BnAO. Although cellular reductase enzymes and other complex factors in vivo may affect the accumulation of Tc–BnAO in hypoxic cell, our calculation results of interconversion mechanism between TcO_2–BnAO and TcO–BnAO are quite useful to further investigate the hypoxic mechanism of Tc–BnAO in vivo. Further works will be undertaken for including the real cellular reductase enzymes in our calculations.

4 Conclusion

According to the above discussions, the following conclusions could be drawn:

The stabilities of formal TcO_2^{+} and TcO^{3+} core are dependent on ring-length of backbone, the longer the ring, the more stable the formal TcO_2^{+} core. The reason for this is that the ring expansion from formal TcO^{3+}–TcO_2^{+} core will affect the hydrogen-bond strength of O…H–O.

The interconversion reaction between formal TcO_2^{+} and TcO^{3+} core includes two distinct addition steps: the addition and proton transfer processes with the aid of water molecules.

The stabilities of TcO–BnAO and TcO_2–BnAO are comparable. The interconversion from TcO–BnAO to TcO_2–BnAO needs to overcome two energy barriers of 10 and 15 kcal/mol, and that the latter is higher might be responsible for the coexistence of TcO–BnAO, TcO(OH)–BnAO and TcO_2–BnAO.

Acknowledgments This work is financially supported by the Research Fund for the Doctoral Program of Higher Education (no. 20040027011) and National Natural Science Foundation of China (nos. 20501004 and 20773016) and the High-Powered Computing Center of Beijing Normal University for partial CPU times.

References

1. Jurisson S, Berning D, Jia W, Ma D (1993) Chem Rev 93:1137. doi:10.1021/cr00019a013
2. Archer CM, Edwards B, Kelly JD, King AC, Burke JF, Riley ALM (1995) In: Nicolini M, Bandoli G, Mazzi U (eds) Technetium and rhenium in chemistry and nuclear medicine. SGE Ditoriali, Padova, p 535
3. Imahashi K, Morishita K, Kusuoka H, Yamamichi Y, Hasegawa S, Hashimoto K et al (2000) J Nucl Med 41:1102
4. Honess DJ, Hill SA, Collingridge DR, Edwards R, Brauers G, Powell NA et al (1998) Int J Radiat Oncol Biol Phys 42:731. doi:10.1016/S0360-3016(98)00300-9
5. Zhang X, Melo T, Ballinger JR, Rauth AM (1998) Int J Radiat Oncol Biol Phys 42:737. doi:10.1016/S0360-3016(98)00301-0
6. Cook GJR, Houston S, Barrington SF, Fogelman I (1998) J Nucl Med 39:99
7. Yutani K, Kusuoka H, Fukuchi K, Tatsumi M, Nishimura T (1999) J Nucl Med 40:854
8. Tatsumi M, Yutani K, Kusuoka H, Nishimura T (1999) Eur J Nucl Med 26:91. doi:10.1007/s002590050364
9. Fair CK, Troutner DE, Schlemper EO, Murmann RK, Hoppe ML (1984) Acta Crystallogr C 40:1544. doi:10.1107/S0108270184008647
10. Jurisson S, Schlemper EO, Troutner DE, Canning LR, Nowotnik DP, Neirinckx RD (1986) Inorg Chem 25:543. doi:10.1021/ic00224a031
11. Walker PS, Bergin PM, Grossel MC, Horton PN (2004) Inorg Chem 43:4145. doi:10.1021/ic0497634
12. Jurisson S, Aston K, Fair CK, Schlemper EO, Sharp PR, Troutner DE (1987) Inorg Chem 26:3576. doi:10.1021/ic00268a031
13. Cyr JE, Nowotnik DP, Pan Y, Gougoutas JZ, Malley MF, Marco JD et al (2001) Inorg Chem 40:3555. doi:10.1021/ic991381o
14. Brauers G, Archer CM, Burke JF (1997) Eur J Nucl Med 24:943
15. Becke AD (1993) J Chem Phys 98:5648. doi:10.1063/1.464913
16. Lee C, Yang W, Parr RG (1988) Phys Rev B 37:785. doi:10.1103/PhysRevB.37.785
17. Frisch MJ, Trucks GW, Schlegel HB, Scuseria GE, Robb MA, Cheeseman JR (2004) Gaussian, Inc., Wallingford CT, Gaussian 03, Revision C.02
18. Bader RFW (1991) Chem Rev 91:893. doi:10.1021/cr00005a013
19. Bader RFW (1990) Atoms in molecules: a quatum theory. Clarendon Press, Oxford
20. Godbout N, Salahub DR, Andzelm J, Wimmer E (1992) Can J Chem 70:560. doi:10.1139/v92-079
21. Hay PJ, Wadt WR (1985) J Chem Phys 82:299. doi:10.1063/1.448975
22. Ishida K, Morokuma K, Komornicki A (1977) J Chem Phys 66:2153. doi:10.1063/1.434152
23. Gonzales C, Schlegel HB (1989) J Chem Phys 90:2154. doi:10.1063/1.456010
24. Gonzales C, Schlegel HB (1990) J Chem Phys 94:5523. doi:10.1021/j100377a021
25. Scott AP, Radom L (1996) J Phys Chem 100:16502. doi:10.1021/jp960976r
26. Young D (2001) Computational chemistry, a practical guide for applying techniques to real world problems. Willey-Interscience, New York
27. Miertus S, Scrocco E, Tomasi J (1981) Chem Phys 55:117. doi:10.1016/0301-0104(81)85090-2
28. Miertus S, Tomasi J (1982) Chem Phys 65:239. doi:10.1016/0301-0104(82)85072-6
29. Cossi M, Barone V, Cammi R, Tomasi J (1996) Chem Phys Lett 255:327. doi:10.1016/0009-2614(96)00349-1
30. Cances MT, Mennucci V, Tomasi J (1997) J Chem Phys 107:3032. doi:10.1063/1.474659
31. Barone V, Cossi M, Mennucci B, Tomasi J (1997) J Chem Phys 107:3210. doi:10.1063/1.474671
32. Cossi M, Barone V, Tomasi J (1998) Chem Phys Lett 286:253. doi:10.1016/S0009-2614(98)00106-7
33. Barone V, Cossi M (1998) J Phys Chem A 102:1995. doi:10.1021/jp9716997
34. Bader RFW, Biegler-König FW, Cheeseman JR, Duke JA, Keith TA, Krug P et al (1994) AIMPAC (a set of programs for the theory of atoms in molecules). McMaster Univeristy, Hamilton
35. Biegler-König FW, Bader RFW, Tang TH (1982) J Comput Chem 3:317. doi:10.1002/jcc.540030306
36. Fang DC, Tang TH (1998) AIM98PC (a modified PC version of AIMPAC). Beijing Normal University, Beijing
37. Biegler-König F, Schonbohm J, Bayles D (2001) J Comput Chem 22:545. doi :10.1002/1096-987X(20010415)22:5<545::AID-JCC1027>3.0.CO;2-Y
38. Biegler-König F, Schonbohm J (2002) J Comput Chem 23:1489. doi:10.1002/jcc.10085
39. Ding WJ, Fang DC (2001) J Org Chem 66:6673. doi:10.1021/jo010461i
40. Wei MJ, Fang DC, Liu RZ (2002) J Org Chem 67:7432. doi:10.1021/jo0258709
41. Yang SY, Sun CK, Fang DC (2002) J Org Chem 67:3841. doi:10.1021/jo025575o
42. Ding YQ, Fang DC (2003) J Org Chem 68:4382. doi:10.1021/jo0340713
43. Zhang X, Melo T, Rauth AM, Ballinger JR (2001) Nucl Med Biol 28:949. doi:10.1016/S0969-8051(01)00267-0